Investigation of SPIO T₁-signature: Positive Contrast using Ultrashort TE Imaging

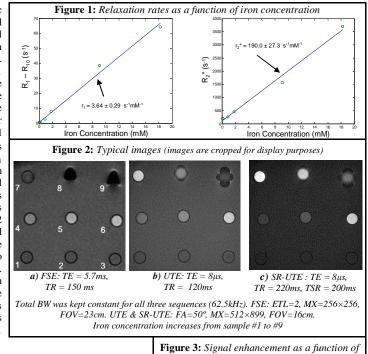
O. M. Girard¹, J. Du¹, and R. F. Mattrey¹

¹Department of Radiology, University of California, San Diego, CA, United States

Purpose: Superparamagnetic iron oxide (SPIO) nanoparticles are efficient contrast agents for molecular and cellular MR imaging [1]. They are usually considered to be negative contrast agents, since their magnetic moment causes signal dephasing which results in signal voids on T₂* weighted images. However SPIO agents also have intrinsic T₁ shortening properties [2] that can induce signal enhancement using appropriate pulse sequences, although these are usually counterbalanced by the T₂* effect at high iron concentrations. Several methodological studies have been done to investigate the balance between those two opposed effects using classical MR pulse sequences [3, 4]. In addition positive contrast methods have been proposed to track SPIO nanoparticles [5, 6]. Those methods rely on susceptibility related effects produced in vicinity of the iron core. Here we propose to investigate the positive contrast due to the T₁ shortening using Utrashort TE (UTE) MR pulse sequences [7]. In addition to usual Ty* contrast one could benefit from the T₁ signature of SPIO agents to improve specificity as well as localization while avoiding misclassification of signal drop out. Potential applications are imaging of inflammation and tumor metastases.

Material and Methods: Sample preparation: In Vitro iron particle homogeneous suspensions were prepared by diluting ferumoxides (Feridex, Bayer HealthCare Pharmaceutical) in 2% agarose gel. Each sample was prepared in a 2 mL cylindrical vial and contained a different SPIO dose (10⁻⁴, 5×10⁻⁴, 10⁻³, 5×10⁻³, 0.01, 0.05, 0.1, 0.5 and 1 mg of iron per mL; corresponding to 1.8×10^3 to 18 mM - Iron mass = 55.85 g/mol). Vials were placed in a plastic container filled with agarose gel in order to avoid susceptibility artifacts from the surrounding air and to assess signal enhancement with respect to the background signal. Another advantage was to have an insight into T2* effects that were not restricted to the inside of each sample (as opposed to T1 effect). MRI: All images were acquired on a 3T clinical system (General Electric) at room temperature. All studied images were obtained with 2D pulse sequences with a 2 mm slice thickness and sample axes perpendicular to B₀. T₁ was evaluated for each iron concentration using either a broadband Saturation Recovery prepared UTE sequence for the four highest iron concentration (SR-UTE: BW=62.5kHz, FOV=16cm, Mx=256x256, TR=500ms, TE=8µs, FA=50° with five saturation times -TSR- ranging from 13.5ms to 100ms) or a regular Inversion Recovery prepared Fast Spin Echo (FSE) for the remaining lower iron concentration (IR-FSE: BW=15.63kHz, FOV=23cm, Mx=256x256, ETL=12, TR=6000ms, TE=11.8ms with seven inversion times -TI- ranging from 70ms to 3600ms). T₂* was assessed using a regular UTE sequence (as opposed to SR-UTE) with twelve echo times ranging from 8µs to 8ms (BW=62.5kHz, FOV=16cm, Mx=256x256, TR=300ms, FA=50°). T1 weighted FSE imaging was performed for comparison. In addition UTE and SR-UTE sequences were performed at various FAs and TRs to assess the effect of different T1 weightings. Data analysis: In all cases, signals were measured by drawing ROIs in the center of each tube. T_1 quantification was performed by fitting the following analytical function $A \times |1 - B \times exp(-T_{recover}/T_1) + C|$ (where $T_{recovery}$ was TSR for SR-UTE or TI for IR-FSE) to the signal recovery curve with A, B, C and T₁ as free parameters. Considering B as a free parameter is an essential feature of this analysis since the actual flip angle may differ from the nominal one (90° for SR ideally corresponds to B=1) when T_2 is of the order of the RF pulse duration [7]. T_2^* were extracted by fitting $D \times exp(-TE/T_2^*) + E$ to the measured signal decay with D, E and T_2^* as free parameters. Offset terms (i.e. C and E) were added to the usual exponential models in order to account for noise or potential artifacts. Both T₁ and T₂* measurements were used to calculate the corresponding relaxivities of the samples. Finally contrast enhancement with respect to the background signal (measured close to the image center) was computed as a function of iron concentration for each of the three different types of sequence (FSE, regular UTE and SR-UTE).

Results and Discussion: T₁ evaluation did not show any evidence of systematic errors. However for the three lowest iron concentration as well as for the background signal, T₂* fitting was of poor quality since the measured signal was not exponential and demonstrated some oscillations at low values of TE. This effect has already been identified with UTE sequences and is a consequence of short term eddy currents [7]. Hence only the six highest concentration data points are reported here. Figure 1 displays measured relaxation rates as a function of the iron concentration. R_{10} is the longitudinal relaxation rate of the background gel. Linear regressions lead to the displayed iron relativities and the corresponding 95% confidence intervals. Those values are in fair agreement with literature values [2, 8] and corresponds to a r2* over r₁ ratio of the order of 52 (at 3T and room temperature). Typical images and corresponding parameters are shown in Figure 2. Among conventional sequences (i.e. non UTE ones) FSE is generally regarded as a good choice to show T₁ weighting while avoiding strong T2* effects. As illustrated in a) for the medium range concentrations, this sequence shows positive contrast. However the signal drops as the iron concentration is increased. Conversely, UTE sequences with 8µs nominal TE have the ability to probe T_1 effect even with very short T_2^* values (measured to be 0.64 and 0.27 ms for the two highest iron concentrations). Figure 2 b) and more particularly c) illustrate this ability, where even the most concentrated samples exhibit positive contrast with respect to the background. Note also the localized T_1 enhancement as compared to the extended T_2^* hyposignal for the two highest concentrations. Figure 3 shows the corresponding quantitative analysis. According to those data a 14% difference is probably not significant since variation of the background signal due to RF inhomogeneity or other causes across the image was observed. Different image contrast was obtained with regular UTE sequences varying its parameters. As a general rule detectability of high iron concentration was better with short TRs and high FAs (related to a corresponding very short T₁). Figure 2 c) displays the best overall contrast obtained.



400%

350%

300% 250%

200%

1009

-50%

-100%

Enhan 150%

Signal [50% 0% iron concentration

0.1

100

- FSE

-O-- UTE

SR-UTE

0.01

Conclusion and Perspectives: UTE sequences have a unique potential to probe signal form tissues and fluids with very short T₂ components. Hence they are of considerable interest for iron oxide nanoparticle imaging and have the potential to improve detection specificity and localization. Here we have demonstrated that a positive contrast is possible for highly concentrated SPIO particles using UTE sequences with an 8µs nominal TE. In particular SR-UTE revealed a contrast pattern that has not been described previously to our knowledge. Other type of sequences such as narrowband off resonance SR-UTE and IR-UTE will be investigated in further work. Positive contrast could also benefit from lower magnetic field strength or smaller SPIO particles since T₁ relaxivity is known to reach an optimum at low field strength (of the order of 0.2T) and r_2/r_1 ratio decreases with the particle size [2]. In vitro iron labeled cells as well as in vivo experiments will be investigated to evaluate compartmentalization related effects [8] and to assess the impact on diagnosis of UTE sequences.

Iron Concentration (mM) References: 1. Corot C, et al. Adv Drug Deliv Rev, 2006, 58: p1471 2. Roch A, et al. J Chem Phys, 1999, 110: p5403 3. Small WC, et al. Magn Reson Imaging, 1993, 11: p645 4. Chambon C, et al. Magn Reson Imaging, 1993, 11: p509 5. Liu W, et al. NMR in Biomed, 2008, 21: p242 6. Cunningham CH, et al. Magn Reson Med, 2005, 53: p999 7. Robson MD, et al. J Comput Assist Tomogr, 2003, 27: p825 8. Bowen CV, et al. Magn Reson Med, 2002, 48: p52